Ultraviolet Photochemistry of Diacetylene: The Metastable C_4H_2* Reaction with Ethene, Propene, and Propyne

Rex K. Frost, Caleb A. Arrington, Christopher Ramos, and Timothy S. Zwier*

Contribution from the Department of Chemistry, Purdue University, West Lafayette, Indiana 47907-1393

Received November 9, 1995[⊗]

Abstract: The chemistry of the triplet metastable state of diacetylene (C_4H_2*) with ethene, propene, and propyne in nitrogen and helium buffers is studied in a reaction tube attached to a pulsed nozzle. An ultraviolet photoexcitation laser counterpropagates the molecular expansion through a short reaction tube, exciting the C_4H_2 $^1\Delta_u \leftarrow {}^1\Sigma_g^+$ $2^1_0 6^1_0$ and 6^1_0 transitions at 231.5 and 243.1 nm, respectively. Efficient intersystem crossing forms the metstable triplet state from which reaction occurs. The short length of the tube (8 mm) serves to quench the reaction after 10−30 μs so that primary products and not polymer are formed. Upon exiting the reaction tube, the photochemical products are soft ionized with 118 nm vacuum ultraviolet light and mass-analyzed in a linear time-of-flight mass spectrometer. The primary products in the reactions with ethene (C_6H_4, C_6H_5), propene (C_5H_5, C_5H_6, C_6H_4, and C_7H_6), and propyne (C_5H_3, C_5H_4, C_6H_2, and C_7H_4) are consistent with poly-yne, enyne, and cumulene products. Percent product yields are determined assuming equal photoionization cross sections for the products. Relative photoionization cross sections at 118 nm for a series of model alkene, alkyne, enyne, diene, and diyne compounds are determined to test the variations in photoionization cross section expected for the products. Relative rate constants for the reactions (scaled to $k(C_4H_2^* + C_4H_2) = 1.00$) with ethene, propene, and propyne are extracted from concentration studies, determining values of 0.24 ± 0.01, 0.32 ± 0.01, and 0.42 ± 0.02 in helium buffer, respectively. Isotopic studies employing deuterated reactants are used to constrain the mechanisms for the reactions. Most of the major products are proposed to follow formation of an unbranched or branched chain adduct which subsequently decomposes by loss of interior atoms to form a stable poly-yne or en-yne product. Two schemes are proposed to account for formation of the isotopically labeled C_5H_4 and C_5H_3 products in the $C_4H_2^* + CH_3C_2H$ reaction. Only one of these mechanisms appears to be operative in the $C_4H_2^* + CH_3CH{=}CH_2$ reaction.

I. Introduction

Diacetylene (C_4H_2) plays a role in diverse areas ranging from planetary atmospheres to sooting flames. The identification of diacetylene in the atmosphere of Titan, one of the moons of Saturn, marks it as the largest photochemically active hydrocarbon so far identified there.[1−5] Diacetylene's near-ultraviolet absorptions are at longer wavelengths than those of most other species in the atmospheres (e.g., CH_4 or C_2H_2), thereby exposing it to photoexcitation by the more intense solar radiation at these wavelengths. The products of diacetylene's photochemical reactions with the other constituents of Titan's atmosphere are expected to have even longer conjugated poly-yne and enyne chains, suggesting them as potential precursors to the visible absorbing haze present in Titan's stratosphere.[3,4] The fate of C_4H_2 in Titan's atmosphere is also important as a route for removal of carbon from the gas phase (by condensation) and potentially as a catalyst for recombining hydrogen atoms to H_2.[3,4] Diacetylene is also thought to play a role in the atmospheres of Uranus,[6−8] Neptune,[9−11] Triton,[12] and to some extent Jupiter[13,14] and Saturn.[15]

Diacetylene is also notable as the most abundant C_4 species in flames, especially under fuel-rich conditions leading to soot formation. In fact, in the burned gas where polycyclic aromatic hydrocarbons (PAHs) are increasing in concentration, diacetylene is rivalled only by C_2H_2 (and CH_4 in alkane flames) as the most abundant light hydrocarbon present.[16−18] C_4H_2 is a precursor to longer-chain poly-yne species, but the further reaction pathways taken by these long-chain species and the mechanism for their incorporation into soot are still under active investigation.

Diacetylene's ultraviolet photochemistry is notable in two respects. First, ultraviolet photoexcitation of C_4H_2 leads to efficient polymer formation. In fact, bulb studies[19] of diacety-

* Author to whom correspondence should be addressed.

⊗ Abstract published in *Advance ACS Abstracts,* April 15, 1996.

(1) Kunde, V. G.; Aiken, A. C.; Hanel, R. A.; Jennings, D. E.; Maguire, W. C.; Samuelson, R. E. *Nature* **1981**, *292*, 686.

(2) (a) Coustenis, A.; Bezard, B.; Gautier, D. *Icarus* **1989**, *80*, 54. (b) Coustenis, A.; Bezard, B.; Gautier, D.; Marten, A.; Samuelson, R. *Icarus* **1991**, *89*, 152.

(3) (a) Yung, Y. L.; Allen, M.; Pinto, J. P. *Astrophys. J. Suppl. Ser.* **1984**, *55*, 465. (b) Yung, Y. L. *Icarus* **1987**, *72*, 468.

(4) Toublanc, D.; Parisot, J. P.; Brillet, J.; Gautier, D.; Raulin, F.; McKay, C. P. *Icarus* **1995**, *113*, 2.

(5) Strobel, D. F.; Summers, M. E.; Zhu, X. *Icarus* **1992**, *100*, 512−526.

(6) Atreya, S. K.; Sandel, B. R.; Romani, P. N. In *Uranus*; Bergstralh, J. T., Ed.; University of Arizona, 1990.

(7) Summers, M. E.; Strobel, D. F. *Astrophys. J.* **1989**, *346*, 495.

(8) Pollack, J. B.; Rages, K.; Pope, S. K.; Tomasko, M. G.; Romani, P. N.; Atreya, S. K. *J. Geophys. Res.* **1987**, *92*, 15,037.

(9) (a) Romani, P. N.; Atreya, S. K. *Icarus* **1988**, *74*, 424. (b) Romani, P. N.; Atreya, S. K. *Geophys. Res. Lett.* **1989**, *16*, 941. (c) Romani, P. N.; Bishop, J.; Bezard, B.; Atreya, S. *Icarus* **1993**, *106*, 442.

(10) Moses, J. I.; Allen, M.; Yung, Y. L. Icarus **1992**, *99*, 318−346.

(11) Yelle, R. V.; Herbert, F.; Sandel, B. R.; Vervack, R. J.; Wentzel, T. M. *Icarus* **1993**, *104*, 38.

(12) Cruikshank, D. P.; Roush, T. L.; Owen, T. C.; Geballe, T. R.; deBergh, C.; Schmitt, B.; Brown, R. H.; Bartholemew, M. J. *Science* **1993**, *261*, 742.

(13) West, R. A.; Strobel, D. F.; Tomasko, M. G. *Icarus* **1986**, *65*, 161.

(14) Landry, B.; Allen, M.; Yung, Y. L. *Icarus* **1991**, *89*, 377−383.

(15) Karkoschka, E.; Tomasko, M. G. *Icarus* **1993**, *106*, 428−441.

(16) Bastin, E.; Delfau, J.-L.; Reuillon, M.; Vovelle, C.; Warnatz, J. *Symp. Combust.* **1988**, *22*, 313.

(17) (a) Miller, J. A.; Melius, C. F. *Combust. Flame* **1992**, *91*, 21. (b) Melius, C. F.; Miller, J. A.; Evleth, E. M. *Symp. Combust.* **1992**, *24*, 621.

(18) Lam, F. W.; Howard, J. B.; Longwell, J. P. *Symp. Combust.* **1988**, *22*, 323.

S0002-7863(95)03757-7 CCC: $12.00

lene's photochemistry have been unable to detect gas-phase products due to the subsequent polymerization. Second, diacetylene's ultraviolet photochemistry occurs out of a metastable excited state (denoted here as C_4H_2*) rather than via a free radical following photodissociation.[19−23] Glicker and Okabe[19] have determined a photochemical quantum yield of $\phi = 2.0 \pm 0.5$ for the disappearance of diacetylene excited throughout the wavelength range 147−254 nm. Free radical formation is not observed under the conditions of their experiment over the range from 254 to 184 nm, with an upper limit on the quantum yield for C_4H formation of 0.06 at 228 nm. At the same time, the metastable state(s) of C_4H_2 (the $T_1(^3\Sigma_u^+)$ and/or $T_2(^3\Delta_u)$ states) are highly resistant to electronic deactivation by rare gases, nitrogen, and hydrogen, with no quenching observed under conditions in which C_4H_2* suffers thousands of collisions with nonreactive buffer gases.[19]

Our group[21−23] has recently developed a general and versatile laser-based pump-probe scheme for studying the photochemistry of highly reactive molecules like C_4H_2. By attaching a small reaction tube to the end of a pulsed valve and exciting the C_4H_2 during the reaction mixture's traversal of this tube, C_4H_2* is formed and allowed to react for about 20 μs before the reaction is quenched as the gas mixture expands from the tube into the vacuum chamber. The reaction products produced are then photoionized with 118-nm radiation (10.5 eV) and mass-analyzed using time-of-flight mass spectroscopy. In this way, primary products are observed with little interference from the larger polymerization products which would be formed if reaction were allowed to proceed further.

Previous studies employing these methods[21−23] have focussed on the C_4H_2* + C_4H_2 and C_4H_2* + C_2H_2 reactions. In the former reaction, three primary pathways are observed:

$$C_4H_2^* + C_4H_2 \rightarrow C_6H_2 + C_2H_2 \quad (1a)$$

$$\rightarrow C_8H_2 + 2H\,(H_2) \quad (1b)$$

$$\rightarrow C_8H_3 + H \quad (1c)$$

In the latter reaction, C_6H_2 is the single product observed:

$$C_4H_2^* + C_2H_2 \rightarrow C_6H_2 + 2H\,(H_2) \quad (2a)$$

In the present study, the reactivity of C_4H_2* toward ethene, propene, and propyne is explored. Beside the fact that these molecules are some of the most abundant unsaturated hydrocarbons in Titan's atmosphere,[2−4] they also enable a more thorough evaluation of the types of reactions C_4H_2* can undergo with alkenes and with unsaturated molecules containing alkyl groups. These molecules are observed to undergo a rich set of reactions with C_4H_2* to form a variety of C_5, C_6, and C_7 products.

II. Experimental Section

The experimental apparatus employed in these studies has been described previously.[22] Only a brief description is given here. Diacetylene is excited to various vibronic levels of the $^1\Delta_u$ state using the doubled output of an excimer-pumped dye laser (~0.5 mJ/pulse doubled output). This photoexcitation laser counterpropagates the molecular expansion through a ceramic reaction tube (2 mm i.d. × 8 mm long) attached to the end of the pulsed valve. Typical peak powers of 1×10^{10} W/m^2 are used, exciting a few percent of the C_4H_2 in the reaction mixture. Intersystem crossing produces metastable C_4H_2* from which reaction occurs with the reactant of choice during the traversal of the reaction tube. The collision frequency in the reaction tube is sufficient to produce detectable photochemical products, but subsequent reaction is quenched by expansion into the vacuum chamber after only 20 μs so that primary products and not polymer are observed. Typical operating conditions employ a total gas throughput of 3×10^{-3} Pa·m^3·s^{-1}, a piezoelectric pulsed valve pulse width of 300 μs, and a repetition rate of 20 Hz. The estimated total pressure of the reaction mixture in the reaction tube during the gas pulse is about 2.5 mbar while background pressures in the photoionization and time-of-flight chambers with gas flow are 1×10^{-5} and 5×10^{-7} mbar.

Upon exiting the reaction tube, the photochemical products are soft ionized with vacuum ultraviolet (VUV) light at 118 nm (10.5 eV) produced by tripling 355-nm light from a pulsed Nd:YAG laser in xenon gas.[24] Photoionization occurs 8 cm downstream from the reaction tube between the first stage ion source acceleration plates, approximately 70 μs after photoexcitation. The ions so produced are mass analyzed in a linear time-of-flight mass spectrometer and detected using either a microchannel plate (R.M. Jordan) or a microsphere plate ion detector (El-Mul Technologies).

Several types of spectra are reported in this study, and are explained in more detail elsewhere.[22,23] Difference mass spectra highlight photochemical products by subtracting background mass spectra obtained with the photoexcitation laser present. Action spectra are recorded by monitoring photoproduct ion intensities as a function of photoexcitation wavelength. Reaction time scans of photoproducts result from maintaining a constant delay between the pulsed valve opening and the ionization laser while varying the delay between the photoexcitation laser and the VUV laser. Finally, concentration studies measure the total integrated intensities of the product peaks as a function of the $[C_nH_m]/[C_4H_2]$ concentration ratio in the reaction mixture.

The synthesis and handling of diacetylene have been described previously.[22] Isotopically pure C_4D_2 is prepared by following the C_4H_2 synthesis of Armitage et al.,[25] substituting D_2O and NaOD in the reaction. This procedure led to product that was not fully deuterated, creating an approximately equal mixture of C_4H_2, C_4HD, and C_4D_2. Complete deuterium exchange is accomplished with the addition of two deuterium washing stages, consisting of 10 mL of 10% NaOD in D_2O. The diacetylene was bubbled through these stages prior to cold finger trapping. An impurity always present in the synthesis of C_4H_2, 2-chloro-1-butene-3-yne (M/Z = 86, 88), was likewise partially deuterated in this synthesis, leading to impurity peaks at m/z = 87, 89, and 91 when the C_4D_2 was used.

Variable concentration reactant mixtures are prepared in a gas handling system by combining metered flows of 2−4% C_4H_2/He (or C_4H_2/N_2, C_4D_2/He) and ethene, propene, or propyne gas. Ethene (98.5% pure, Airco), propene (99% pure, Airco), and propyne (98%, Farchan) were used as purchased. C_2D_4, CH_3C_2D, CD_3C_2H, and $CD_3CD{=}CD_2$ were purchased (CDN Isotopes) as 0.5-L samples and were also used without further purification. This provided sufficient sample only for studies of the isotopically substituted photochemical products, so that kinetic studies were not attempted with the deuterated gases.

III. Reaction Scheme

In our recent work on the C_4H_2* + C_2H_2 reaction,[23] we introduced a simple reaction scheme which was used in obtaining an effective rate constant for the reaction relative to C_4H_2* + C_4H_2. Here we briefly summarize the scheme as applied to a general reaction and state its predicted consequences.

(19) Glicker, S.; Okabe, H. *J. Phys. Chem.* **1987**, *91*, 437.
(20) Bandy, R. E.; Lakshminarayan, C.; Zwier, T. S. *J. Phys. Chem.* **1992**, *96*, 5337.
(21) Bandy, R. E.; Lakshminarayan, C.; Frost, R. K.; Zwier, T. S. *Science* **1992**, *258*, 1630.
(22) Bandy, R. E.; Lakshminarayan, C.; Frost, R. K.; Zwier, T. S. *J. Chem. Phys.* **1993**, *98*, 5362.
(23) Frost, R. K.; Zavarin, G. S.; Zwier, T. S. *J. Phys. Chem.* **1995**, *99*, 9408−9415.
(24) Mahon, R.; McIlrath, T. J.; Myerscough, V. P.; Koopman, D. W. *IEEE J. Q. Electronics* **1979**, *6*, 444−451.
(25) Armitage, J. B.; Jones, E. R. H.; Whiting, M. C. *J. Chem. Soc.* **1952**, 2014.

The experimental method probes the early-time course of these reactions. By initiating the reaction with a laser pulse, allowing it to proceed for about 20 μs, and quenching the reaction as the gas mixture expands into the vacuum, secondary reactions have been experimentally demonstrated to occur to a negligible extent. This is a major advantage of the present method for studying these reaction mixtures which have the potential for extensive polymerization under bulb or flow tube conditions.

When applied to a reaction mixture containing C_4H_2 and a reactant hydrocarbon C_nH_m, the reaction scheme is:

$$C_4H_2 + h\nu \rightarrow {}^1C_4H_2^*$$

$${}^1C_4H_2^* \rightarrow {}^3C_4H_2^*$$

$$\begin{aligned} {}^3C_4H_2^* + C_4H_2 &\rightarrow C_6H_2 + C_2H_2 && k_{1a} \\ &\rightarrow C_8H_2 + 2H\ (H_2) && k_{1b} \\ &\rightarrow C_8H_3 + H && k_{1c} \\ {}^3C_4H_2^* + C_nH_m &\rightarrow \text{Prod(2a)} && k_{2a} \\ &\rightarrow \text{Prod(2b)} && k_{2b} \\ &\vdots \end{aligned}$$

The intersystem crossing to the triplet state is written as an intramolecular process which is fast compared to all other processes, as suggested by the lifetime broadening of the transitions being pumped.[20] The detailed route to formation of the metastable state is not included explicitly in the reaction scheme, nor is it known. For the purposes of the kinetic scheme, we simply treat the metastable state as a single entity out of which reaction occurs.

Vibrational deactivation within the triplet manifold is also not explicitly included in the scheme. Since such deactivation occurs in parallel with reaction, the rate constants derived are thus effective rate constants. Their values can vary with the nature of the buffer gas (e.g., helium versus N_2) by changing the internal energy distribution of the reacting $C_4H_2^*$.

Given this simple scheme, the time-dependent concentration of any one of the products is just:

$$[\text{Prod(2a)}] = \left\{\frac{k_{2a}[C_nH_m][C_4H_2^*]_o}{k_1[C_4H_2] + k_2[C_nH_m]}\right\} \times \{1 - \exp(-(k_1[C_4H_2] + k_2[C_nH_m])t)\} \quad (3)$$

where k_1 and k_2 are total reaction rate constants.

The obvious prediction of the reaction scheme is that all primary products of the $C_4H_2^*$ chemistry should have the same time dependence. Furthermore, at all times t,

$$\frac{\sum_i [\text{Prod}(2i)]}{\sum_j [\text{Prod}(1j)]} = \left(\frac{k_2}{k_1}\right)\left(\frac{[C_nH_m]}{[C_4H_2]}\right) \quad (4)$$

so that a plot of the left-hand side of eq 4 versus $[C_nH_m]/[C_4H_2]$ should yield a straight line of slope (k_2/k_1).

In the present experiment, we measure not concentrations directly but product ion signals following photoionization. The ion intensity associated with the product of reaction 2a is given by:

$$I(\text{Prod(2a)}) = \phi_{\text{coll}}\sigma_{\text{PI}}(2a)P_{\text{laser}}[\text{Prod(2a)}] \quad (5)$$

where ϕ_{coll} is the collection efficiency of the product, $\sigma_{\text{PI}}(2a)$ is its photoionization cross section at 118 nm, and P_{laser} is the 118 nm laser power. Under conditions of constant laser power and collection efficiency for all products,

$$\frac{\sum_i I(2i)}{\sum_j I(1j)} = \left(\frac{\sum_i k_{2i}\sigma_{\text{PI}}(2i)}{\sum_j k_{1j}\sigma_{\text{PI}}(1j)}\right)\left(\frac{[C_nH_m]}{[C_4H_2]}\right) = \left(\frac{k_2}{k_1}\right)\left(\frac{[C_nH_m]}{[C_4H_2]}\right) \quad (6)$$

so that a linear plot of the left-hand side of (6) versus $[C_nH_m]/[C_4H_2]$ is predicted. The slope of this plot gives the rate constant ratio k_2/k_1 if the photoionization cross sections of the products are equal.

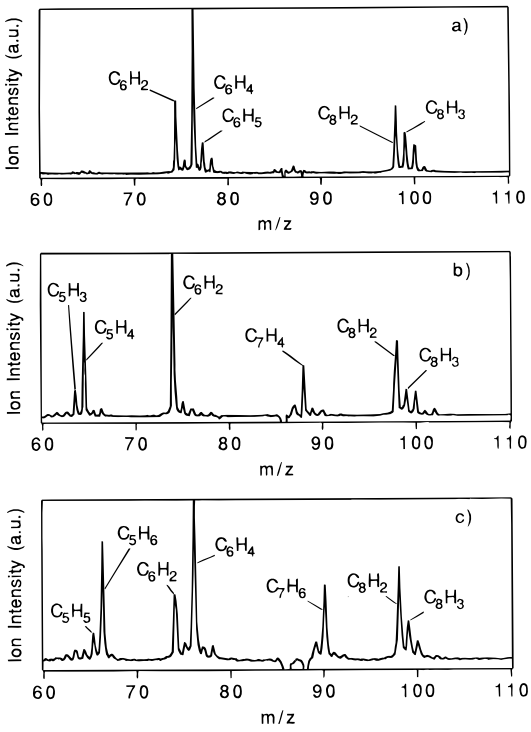

Figure 1. Difference time-of-flight mass spectra highlighting the primary photoproducts of the reactions (a) $C_4H_2^* + C_2H_4$, (b) $C_4H_2^* + CH_3C_2H$, and (c) $C_4H_2^* + CH_3CHCH_2$. The reaction mixtures used are 3% C_4H_2, 9−15% C_nH_m, and the balance helium. The metastable excited state of diacetylene is prepared by pumping the ${}^1\Delta_u\ 2^1_0 6^1_0$ transition at 231.5 nm, followed by intersystem crossing to form the triplet state. The $C_4H_2^+$ peak (not shown) is about 200 times the size of the product peaks.

IV. Results and Analysis

A. Characterization of the Photochemical Reactions. 1. Difference Mass Spectra after $2^1_0 6^1_0$ Excitation. Figures 1a−c present the difference time-of-flight (TOF) mass spectra following excitation of the $2^1_0 6^1_0$ band of the ${}^1\Delta_u \leftarrow {}^1\Sigma_g^+$ transition of C_4H_2 in the presence of ethene, propyne, and propene, respectively. The reaction mixture conditions are given in the figure caption. The $C_4H_2^* + C_nH_m$ product peaks marked in the scans are those due to the reactions of interest. The low-mass regions of the propyne and propene reactions (not shown) also have product peaks due to methyl radical ($m/z = 15$). The $C_4H_2^* + C_4H_2$ products (C_6H_2, C_8H_2, C_8H_3, and C_8H_4) are also

present in all the spectra since this reaction necessarily occurs in parallel with the reactions of interest.

The negative-going peaks at masses 86 and 88 are due to 2-chloro-1-butene-3-yne, a side-product of the synthesis of C_4H_2. It is present in the gas mixture at a concentration of 1−2% that of C_4H_2. Its imperfect subtraction in the difference TOFMS has been addressed in previous publications.[22,23] Arguments will be given in Section A.7 that this impurity is not involved in the observed diacetylene photochemistry.

Based on the masses of the C_nH_m products, the molecular formulae of the observed products can be deduced, and are given in the figure. The reactions corresponding to these product peaks are given below:

Ethene:

$$C_4H_2^* + C_2H_4 \rightarrow C_6H_4 + (2H), (H_2) \quad (7a)$$

$$\rightarrow C_6H_5 + H \quad (7b)$$

Propyne:

$$C_4H_2^* + CH_3C{\equiv}CH \rightarrow C_7H_4 + (2H), (H_2) \quad (8a)$$

$$\rightarrow C_6H_2 + CH_3 + (H), (CH_4) \quad (8b)$$

$$\rightarrow C_5H_4 + (C_2H_2) \quad (8c)$$

$$\rightarrow C_5H_3 + (C_2H_2 + H) \quad (8d)$$

Propene:

$$C_4H_2^* + CH_3CH{=}CH_2 \rightarrow C_7H_6 + (2H), (H_2) \quad (9a)$$

$$\rightarrow C_6H_4 + CH_3 + (H), (CH_4) \quad (9b)$$

$$\rightarrow C_5H_6 + (C_2H_2) \quad (9c)$$

$$\rightarrow C_5H_5 + (C_2H_2 + H) \quad (9d)$$

The species in parentheses are not observed directly because they have ionization potentials greater than 10.5 eV. Note that in the case of reactions (8b) and (9b), both the C_6H_n and CH_3 products are observed. However, CH_4 is not detected, so that its presence cannot be excluded. The C_2H_2 product is also not observed directly; however, the corresponding $C_2H + H$ channel is endothermic at the excitation wavelength used, nor is C_2H observed. Reactions 8d and 9d are written assuming loss of $C_2H_2 + H$ rather than C_2H_3. The latter product, if formed, should be detectable with 10.5-eV photons, but is not observed.

It should be noted that all observed products can be formed in a single $C_4H_2^* + C_nH_m$ reactive collision; that is, no products more complex than C_6 or C_7 are detected in the reactions with C_2H_4, C_3H_4, and C_3H_6. This supports the contention that the observed products are the primary products from $C_4H_2^* + C_nH_m$.

The translation of the observed ion signals into percent product yields requires a knowledge of the relative photoionization cross sections of the products, an issue to be taken up in the Discussion section. However, the remarkable similarity of the propene and propyne results is worth noting immediately. A simple translation of the $C_4H_2^*$ + propyne TOFMS upward by two mass units allows it to be virtually superimposed on the $C_4H_2^*$ + propene product mass spectrum.

2. Action Spectra. Figure 2a presents the R2PI spectrum of the reactant C_4H_2 in the $2^1_0 6^1_0$ region of the $^1\Delta_u \leftarrow {}^1\Sigma_g^+$ transition, while Figure 2b is a representative action spectrum of the C_6H_4 product in the $C_4H_2^* + C_2H_4$ reaction. The action spectrum is produced by tuning the ultraviolet photoexcitation laser through the $2^1_0 6^1_0$ region of C_4H_2 while monitoring product ion signals. The $2^1_0 6^1_0$ transition of C_4H_2 at 231.5 nm and a weak satellite band at 230.5 nm in the R2PI spectrum[20] are both reproduced by the action spectrum. Analogous spectra of all product channels of reactions (7−9) give similar profiles. The reproduction of the diacetylene absorption spectrum by the photoproducts confirms that formation of the observed products follows exclusively from absorption of an ultraviolet photon by gas-phase C_4H_2.

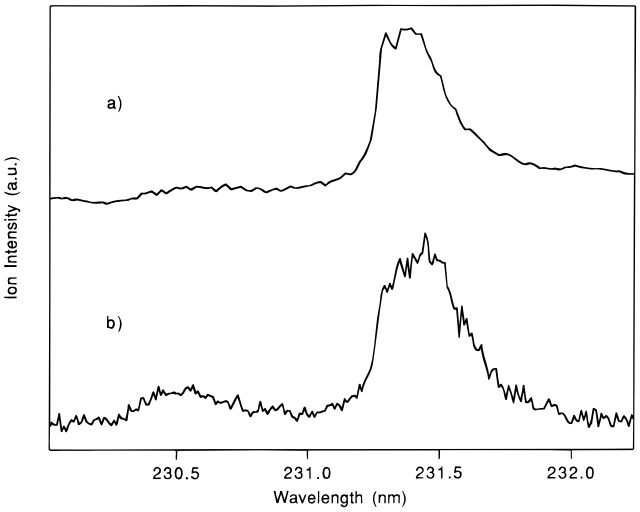

Figure 2. (a) Resonant two-photon ionization spectrum of the reactant C_4H_2 in the $2^1_0 6^1_0$ region near 231 nm. (b) A representative action spectrum of the C_6H_4 product in the $C_4H_2^* + C_2H_4$ reaction, confirming that the C_6H_4 product is only formed following resonant absorption of an ultraviolet photon by gas-phase C_4H_2.

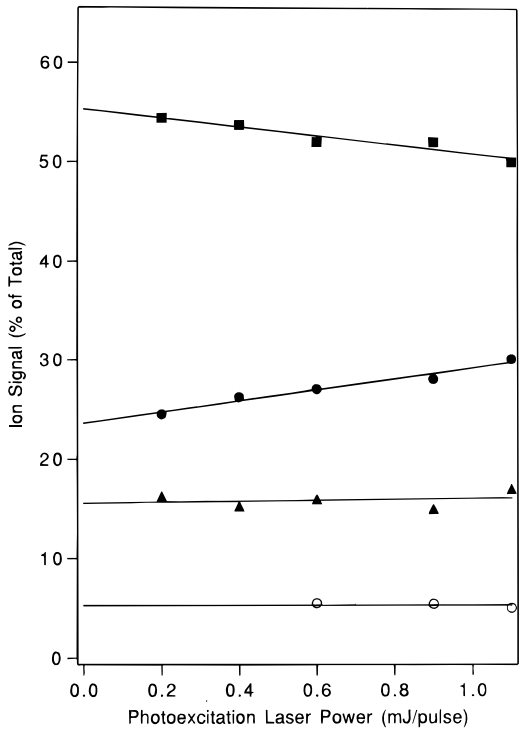

Figure 3. Laser power dependence of the percent yields of the products of the reaction $C_4H_2^*$ + propene.

3. Photoexcitation Laser Power Study. Figure 3 summarizes a representative study of the dependence of the relative product yields on photoexcitation laser power, this time using the $C_4H_2^*$ + propene reaction as the example. Due to

Table 1. Percent Product Photoionization Signals and Effective Relative Rate Constants for the $C_4H_2^* + C_nH_m$ Reactions Studied To Date

$C_4H_2^*$ reaction partner	product	percent product ion signal[a]		effective reaction rate constants[b] relative to $C_4H_2^* + C_4H_2$	
		helium	nitrogen	helium	nitrogen
C_2H_2	C_6H_2	100	100	0.09 ± 0.01	0.15 ± 0.01
C_2H_4	C_6H_4	82 (63)	79	0.24 ± 0.01	0.20 ± 0.01
	C_6H_5	18 (37)	21		
$CH_3CH{=}CH_2$	C_5H_5	6 (5)	6		
	C_5H_6	28 (24)	28	0.32 ± 0.01	0.35 ± 0.02
	C_6H_4	45 (55)	46		
	C_7H_6	21 (16)	20		
$CH_3C{\equiv}CH$	C_5H_3	10 (15)	12		
	C_5H_4	36 (29)	34	0.42 ± 0.02	0.31 ± 0.02
	C_6H_2	28 (36)	32		
	C_7H_4[c]	26 (20)	22		

[a] Percent products were determined with both helium and nitrogen as buffer gases. The percent photoion signals can be interpreted as relative percent yields for the products under the assumption of equal photoionization cross sections for the products at 118 nm. See Section IV.A for further discussion. The numbers in parentheses are percent product yields extrapolated to zero laser power. Errors in individual entries are ±5%. [b] Assuming equal photoionization cross sections for the products. The determinations were carried out under the same laser power conditions as the percent product ion signals listed without parentheses. Quoted errors in the relative rate constants are one standard deviation on the slope from the concentration study and do not include possible contributions to the error from systematic sources such as laser power dependence of the product signals or unequal photoionization cross sections of the $C_4H_2^* + C_nH_m$ and $C_4H_2^* + C_4H_2$ products. [c] Estimated value due to interference from the mass 86 impurity.

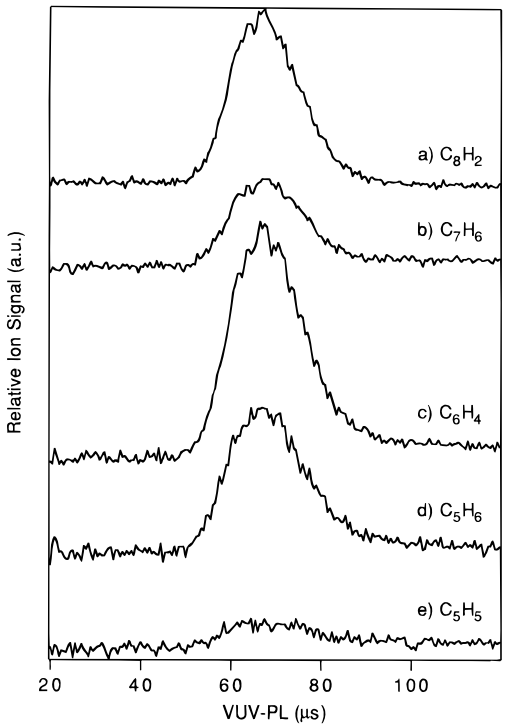

Figure 4. The reaction time profiles of the (a) C_8H_2 product from the $C_4H_2^* + C_4H_2$ reaction and the (b) C_7H_6, (c) C_6H_4, (d) C_5H_6, and (e) C_5H_5 products of the $C_4H_2^*$ + propene reaction following 231.5-nm excitation. The time axis is the delay between the firing of the photoexcitation laser (PL) and the VUV laser with constant delay between the pulsed valve (PV) opening and VUV laser.

instabilities in the VUV source, absolute photoexcitation laser power studies are difficult to conduct over extended time periods. Instead, Figure 3 plots relative product yields of the major products as a function of photoexcitation laser power. Changes in the product distribution with laser power are about 5%, and extrapolation can readily be made to zero laser power conditions. Only in the case of the $C_6H_5 + H$ and $C_6H_4 + 2H$, H_2 product channels are the changes larger (19%, see Table 1), showing a systematic increase in the percent C_6H_5 product at lower laser powers. This suggests that at lower laser powers, the C_6H_5 product formed has lower average internal energy upon formation, and is more easily stabilized relative to loss of a second hydrogen atom to form C_6H_4. The source of this change is likely the higher temperature of the gas mixture at higher laser powers due to the larger energy absorbed by the gas mixture. A similar interplay between $C_8H_2 + 2H$ and $C_8H_3 + H$ products from the $C_4H_2^* + C_4H_2$ reaction is also observed, likely for the same reason.

4. Reaction Time Scans. The reaction time profiles of all significant products of the $C_4H_2^*$ + propene reaction are presented in Figure 4. Reaction time scans are produced by monitoring product ion signal while varying the delay between the firing of the photoexcitation laser (PL) and the VUV laser with constant delay between the pulsed valve (PV) opening and VUV laser. Qualitatively, increasing (VUV-PL) at constant (VUV-PV) is equivalent to increasing the average reaction time of the $C_4H_2^*$ by changing the average position in the reaction tube of the $C_4H_2^*$ whose products are being monitored.

The width of the product signals confirms that the products are formed in reaction times of about 20 μs, consistent with the expected flow velocity down the reaction tube ($\sim 1 \times 10^5$ cm/s). For comparison, the C_8H_2 product from $C_4H_2^* + C_4H_2$ is also presented in Figure 4a. Given the approximate total pressure in the reaction tube, the $C_4H_2^*$ experiences about 300 collisions with buffer gas and 30 collisions with C_nH_m reactant during its traversal of the reaction tube.

Clearly, all the $C_4H_2^*$ + propene products are formed with the same reaction time profile. Analogous scans of the $C_4H_2^*$ reactions with ethene and propyne show identical time dependences. The localization of products in a 20 μs time window indicates that products are not formed on or delayed by interactions with the walls of the reaction tube. Furthermore, the fact that none of the reaction time profiles show a clear induction period, as observed for the C_8H_4 product of $C_4H_2^* + C_4H_2$ (not shown), is consistent with the observed products being primary products of $C_4H_2^* + C_nH_m$ chemistry. Finally, the identical time dependences of the observed products provides confirming evidence that the experimental method views only the early stages of reaction before significant secondary processes have occurred.

5. Reaction in the Presence of N_2. The effect of N_2 on the $C_4H_2^* + C_nH_m$ chemistry has also been studied. N_2 is known from the work of Glicker and Okabe[19] to be an inefficient electronic quencher of metastable $C_4H_2^*$. However, N_2 will vibrationally deactivate metastable $C_4H_2^*$ more efficiently than helium, thereby shifting the internal energy distribution of the reactant $C_4H_2^*$ to lower energies nearer the origin of the metastable $^3\Delta_u$ and/or $^3\Sigma_u^+$ states. In a prior study[21,22] of the $C_4H_2^* + C_4H_2$ reaction, this vibrational deactivation manifested itself in a transfer of product intensity from C_8H_2 to C_8H_3 products (reaction 1b vs 1a). In the present case, however, no significant change in either the nature or distribution of products was observed in the reactions of $C_4H_2^*$ with ethene, propene, or propyne when N_2 was substituted for helium as buffer gas.

6. Dependence of the Products on the Initial Excitation Energy. The majority of the photochemical studies were carried out using excitation of C_4H_2 at 231.5 nm via the $2^1_0 6^1_0$ transition,

123 kcal/mol above the C_4H_2 ground state. However, difference TOFMS were also recorded following excitation at 243.1 nm via the 6^1_0 transition, corresponding to 117.5 kcal/mol excitation energy. For each of the reactions, the difference TOFMS following 6^1_0 excitation (not shown) confirm the presence of the same major products in the same relative intensities as at $2^1_0 6^1_0$.[26]

The 6^1_0 spectra probe the dependence of the product distribution on the initial internal energy of the C_4H_2* and check for contributions from C_4H reactions formed following photodissociation of C_4H_2. Unfortunately, no accurate experimental value for the C−H bond strength in C_4H_2 is available. However, the recent experimental determination[27] of the C−H bond energy in C_2H_2 gives $D_0 = 131.5 \pm 0.7$ kcal/mol. Furthermore, the best current theoretical estimate[28] for $C_4H_2 \rightarrow C_4H + H$ gives an enthalpy change of 133 kcal/mol, corresponding to a 218-nm threshold for C_4H formation. Thus, the lack of change in the major product channels is consistent with the assumption that excitation at both 243.1 and 231.5 nm is well below the threshold for $C_4H + H$ formation. Finally, the insensitivity of the major products to C_4H_2* internal energy probably reflects the modest range of energies explored (5 kcal/mol out of 123).

7. Further Checks on the C_4H_2* Chemistry. The rich variety of products formed in the reactions of C_4H_2* with ethene, propene, and propyne raises certain issues regarding the experimental method.

First, the experimental method is designed to minimize the contribution from secondary reactions. In keeping with this, under most operating conditions, no peaks from C_nH_m products larger than that which can be formed in a single C_4H_2* + C_nH_m collision are observed. In addition, the observed linear dependence of the product signals on the $[C_nH_m]/[C_4H_2]$ concentration ratio (Section B) is consistent with a reaction mechanism in which secondary reactions are negligible.

Second, we have assumed that photoionization exclusively produces the molecular ion without fragmentation. To garner support for the assumption, six unsaturated hydrocarbons with ionization potentials ranging from 9.07 to 10.36 eV were photoionized with 118-nm light (10.5 eV). In all cases, the molecular ion was formed exclusively upon photoionization. Since most of the photochemical products have molecular formulae corresponding to stable, closed-shell molecules, they should also experience negligible fragmentation upon photoionization. Furthermore, a scenario in which one of the smaller mass ions is a photoion fragment of a larger-mass product does not stand up to scrutiny. For instance, in the C_4H_2* + CH_3C_2H reaction, the $C_5H_4^+$ ion differs from the larger products (C_6H_2, C_7H_4) by molecular fragments which cannot easily be lost. Even in the case of the $C_5H_3^+$ ion, which could be formed by fragmentation of $C_5H_4^+$, isotopic data (Section C) indicate that it is not so produced.

A third concern is to determine whether the C_4H_3Cl impurity (mass 86/88) present in the C_4H_2 sample affects the observed product distribution in any way. Extensive attempts to completely remove this impurity from the sample have proved unsuccessful; however, conditions have been found under which C_4H_3Cl is present at about 1% relative to C_4H_2. The action spectra (Figure 2) indicate that the observed products are produced following formation of C_4H_2*, so that direct excitation of C_4H_3Cl as a source of products is ruled out. Furthermore, no undeuterated products are observed in the C_4H_2* + C_nD_m reactions, as would be produced from C_4H_2* + C_4H_3Cl reaction, nor is Cl incorporated in any of the products. Finally, no difference in the product distribution is observed with large changes in C_4H_3Cl concentration in the sample, indicating that the C_4H_3Cl impurity is not contributing to the observed products.

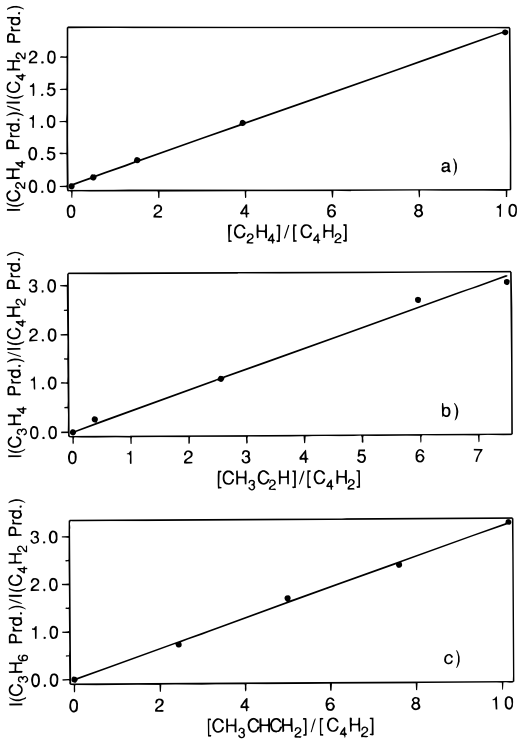

Figure 5. Photoproduct ion intensity ratios $I(C_nH_m$ products$)/I(C_4H_2$ products) plotted versus reactant concentration ratios $[C_nH_m]/[C_4H_2]$. $[C_4H_2$ products$]$ corresponds to the ion intensity sum $I(C_6H_2) + I(C_8H_2) + I(C_8H_3)$ and $[C_nH_m$ products$]$ corresponds to the summed ion intensities for the products of each reaction listed in Table 1. Contributions from the reactions C_4H_2* + C_4H_2 and C_4H_2* + CH_3C_2H to C_6H_2 ion intensity are separated using the observed $[C_6H_2]/([C_8H_2] + [C_8H_3])$ ratio in the absence of CH_3C_2H.

B. Concentration Studies. In Figure 5a−c, the ratio of the integrated intensity of C_4H_2* + C_nH_m product signals relative to those for C_4H_2* + C_4H_2 are plotted as a function of the C_nH_m/C_4H_2 concentration ratio for ethene, propyne, and propene, respectively. Both helium and nitrogen buffers are examined, but only the helium data are included in Figure 5 for clarity. For all three reactions over a wide range of concentrations the intensity ratio varies linearly with $[C_nH_m]/[C_4H_2]$ in both helium and N_2. The linear dependence of $[C_nH_m]/[C_4H_2]$ is consistent with the reaction scheme of Section III, providing further confirmation that secondary reactions are insignificant under the present experimental conditions.

In order to extract rate constants from such a plot, the ion intensities must be transformed into product concentrations. This will be taken up in the Discussion section.

C. Reaction Mechanism: Isotope Studies. In order to obtain further insight to the mechanisms for the C_4H_2* + C_nH_m reactions, difference TOFMS were recorded with a number of deuterium-substituted reactants. Figures 6a−6c present a representative series of difference TOFMS for the C_4H_2* + C_2H_4, C_4D_2* + C_2H_4, and C_4H_2* + C_2D_4 reactions, respectively. Analogous spectra for the isotopic combinations C_4H_2* + $CH_3CH{=}CH_2$, C_4D_2* + $CH_3CH{=}CH_2$, and C_4H_2* + $CD_3CD{=}CD_2$ have also been recorded, as have the series C_4H_2* + CH_3C_2H, C_4D_2* + CH_3C_2H, C_4H_2* + CH_3C_2D, and C_4D_2* + CH_3C_2D

(26) Due to lower laser power and a smaller absorption cross section, the intensities of the minor product channels (<10%) following 6^1_0 excitation cannot be determined with certainty.

(27) Ervin, K. M.; Gronert, S.; Barlow, S. E.; Gilles, M. K.; Harrison, A. G.; Bierbaum, V. M.; DePuy, C. H.; Lineberger, W. C.; Ellison, G. B. *J. Am. Chem. Soc.* **1990**, *112*, 5750−5759.

(28) Kiefer, J. H.; Sidhu, S. S.; Kern, R. D.; Xie, K.; Chen, H.; Harding, L. B. *Combust. Sci. Technol.* **1992**, *82*, 101−130.

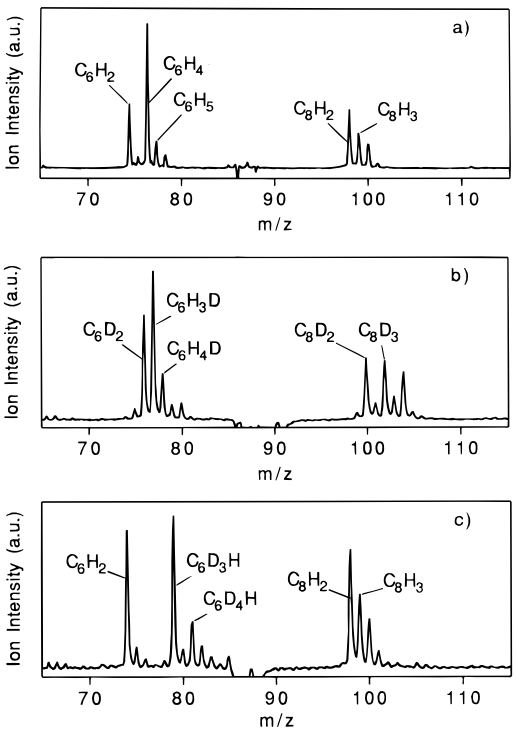

Figure 6. Difference TOFMS for the (a) C_4H_2* + C_2H_4, (b) C_4D_2* + C_2H_4, and (c) C_4H_2* + C_2D_4 reactions. The diacetylene excitation wavelength is 231.5 nm, and a diacetylene-to-ethene ratio of 1:4 in a He buffer was used in each reaction.

for the propyne reaction. The isotopic data are summarized in Table 2, including the key deductions which can be drawn from them.

V. Discussion

A. Percent Product Yields. The experimental data contained in Figure 1 and Table 1 consist of relative photoionization product signals. In order to obtain the percent product yield for the product *i*, PY(*i*), it is necessary to convert the ion signals to neutral concentrations, i.e.,

$$\mathrm{PY}(i) = \frac{[\mathrm{Prod}(i)]}{\sum_j [\mathrm{Prod}(j)]} \text{ where } [\mathrm{Prod}(i)] = \frac{I_{\mathrm{prod}}(i)}{\sigma_{\mathrm{PI}}(i)}$$

where I_{prod}(i) is the relative photoion intensity for product i and $\sigma_{\mathrm{PI}}(i)$ is its photoionization cross section at 118 nm. The expression assumes that the collection efficiency of all products is similar, i.e., that no significant differences exist in the fraction of product molecules transported from the reaction tube to the photoionization region. Then the single factor needed to determine the percent product yields is a knowledge of the relative photoionization cross sections for the products at 118 nm.

The past studies of C_4H_2* reactions with C_4H_2 and C_2H_2 have side stepped this issue by assuming equal photoionization cross sections for the products.[21−23] This was reasonable in light of the chemical similarity of the products (primarily C_nH_2 polyyne), which argued that such differences in photoionization cross sections would be small.

In the present case, a richer mixture of hydrocarbon products is formed, requiring a closer evaluation of the above assumption. Direct determination of the relative photoionization cross sections for the products is not possible at present since in no case do we yet have a structural determination beyond the mass-to-charge ratio. Furthermore, given the highly unsaturated nature of most of the products, the proposed product molecules are not easily prepared, nor will they be easily handled if prepared.

As a lesser goal, we sought instead to determine the possible variations in photoionization cross sections by preparing known-concentration mixtures of model alkene (propene), alkyne (propyne), diene (1,3-butaidene), diyne (C_4H_2), enyne (2-methyl-1-butene-3-yne), and cumulene (allene) compounds and determining their relative photoionization cross sections at 118 nm. The results of this study are as follows. First, for the model compounds studied, the 118-nm photoionization cross sections vary by a factor of 2.5. Second, the cross sections can be divided into two groups: those molecules possessing a triple bond (diacetylene, propyne, and 2-methyl-1-butene-3-yne) have photoionization cross sections about twice that of those without one (propene, allene, and 1,3-butadiene). Within each subgroup, the variation in cross sections is much smaller. In the group possessing triple bonds, cross sections vary by no more than 20%. Since the proposed structures for all products (Section V.C) are either diyne or enyne structures, the variations in photoionization cross sections are not expected to be large.

As a result, it is a reasonable first approximation to assume equal 118-nm photoionization cross sections for the products. Then the percent ion signals reported in Table 1 can be interpreted as percent product yields for the neutral C_4H_2* + C_nH_m products. The cases in which this assumption seems most suspect are the free radical products (e.g., C_5H_3 and C_5H_5) which may differ in their photoionization efficiency from the closed-shell species. However, these are minor product channels.

The percent product yields listed in Table 1 without parentheses are taken at the same laser powers used in the concentration studies to determine the effective relative rate constants for the reaction (next section). The numbers in parentheses are values taken from an extrapolation to zero laser power from the laser power studies. The differences between these values are typically within the estimated errors of the measurement (±5%) except in the case of the C_6H_4/C_6H_5 yields, which more heavily weight C_6H_5 + H formation over the C_6H_4 + 2H channel at low laser power, as was noted previously. This is likely a temperature effect at the higher laser powers (where more energy is absorbed by the gas mixture) which favors the loss of a second hydrogen from the C_6H_5 product.

B. Relative Rate Constants. Since secondary reactions are largely quenched in the present experimental method, the reaction scheme of Section III predicts a linear plot of the integrated intensities of the products of the C_4H_2* + C_nH_m to C_4H_2* + C_4H_2 reactions as a function of $[C_nH_m]/[C_4H_2]$. The results of Figure 5 indicate that linear plots are indeed obtained for all three reactions. By assuming equal photoionization cross sections, effective relative rate constants for the reactions can be determined using eq 6. Thus, within the limits of this assumption, Table 1 presents the effective rate constant ratio obtained for the various reactions, including all those studied to date. The errors on the reported rate constant ratios represent one standard deviation in the linear plots in Figure 5, and do not include potential systematic errors due to the laser power dependence or unequal photoionization cross sections of the individual products. Also included in the table are effective rate constant ratios using N_2 rather than helium as buffer gas. In the reactions with ethene, propene, and propyne, only small effects are seen in the rate constant ratio with changing buffer gas, probably because the C_nH_m gas is itself a fairly efficient

Table 2. Summary of the Major Photochemical Products from Isotopically Substituted C_4H_2* + C_nH_m Reactions in Helium Buffer

reaction partner	Reaction (formula of RC[a])	mass	major products	percent yield	comments
ethene	C_4H_2* + C_2H_4 (C_6H_6)	76	**C_6H_4** + 2H, H_2	82	
		77	**C_6H_5** + H	18	
	C_4H_2* + C_2D_4 ($C_6H_2D_4$)	79	**C_6HD_3** + H + D, HD	71	RC[a] loses one diacetylene H, one ethene D
		78	$C_6D_2H_2$ + 2D, D_2	3	
		81	**C_6HD_4** + H	22	RC preferentially loses one diacetylene H
		80	$C_6D_3H_2$ + D	4	
	C_4D_2* + C_2H_4 ($C_6H_4D_2$)	77	**C_6H_3D** + H + D, HD	75	RC loses one diacetylene D, one ethene H
		76	C_6H_4 + 2D, D_2		likely small
		78	$C_6H_2D_2$ + 2H, H_2		likely small
		77	**C_6H_4D** + D	19	RC preferentially loses one diacetylene D
		79	$C_6H_3D_2$ + H	6	
propene	C_4H_2* + $CH_3CH{=}CH_2$ (C_7H_8)	65	**C_5H_5** + C_2H_3	6	
		66	**C_5H_6** + C_2H_2	28	
		76	**C_6H_4** + CH_3 + H, CH_4	45	
		90	**C_7H_6** + 2H, H_2	21	
	C_4H_2* + $CD_3CD{=}CD_2$ ($C_7H_2D_6$)	70	**C_5D_5** + C_2H_2D	9	both diacetylene H's lost by C_5
		69	C_5HD_4 + C_2HD_2	<1	
		71	**C_5HD_5** + C_2HD	27	one diacetylene H retained by C_5
		72	C_5D_6 + C_2H_2	2	
		79	**C_6HD_3** + CD_3H	44	
		95	**C_7HD_5** + H + D, HD	13	one diacetylene H, one propene D lost
		94	$C_7H_2D_4$ + 2D, D_2	4	
		96	C_7D_6 + 2H, H_2	1	
	C_4D_2* + $CH_3CH{=}CH_2$ ($C_7H_6D_2$)	65	**C_5H_5** + C_2HD_2	10	both diacetylene D's lost by C_5
		66	C_5H_4D + C_2H_2D	5	
		67	**C_5H_5D** + C_2HD	35	one diacetylene D retained by C_5
		77	**C_6H_3D** + CDH_3	27	
		76	C_6H_4 + CD_2H_2		likely small/C_6D_2 interference
		78	$C_6H_2D_2$ + CH_4	<3	
	C_7 products have interference from deuterated impurities; assume ~20%				
propyne	C_4H_2* + $CH_3C{\equiv}CH$ (C_7H_6)	63	**C_5H_3** + C_2H_3	10	
		64	**C_5H_4** + C_2H_2	36	
		74	**C_6H_2** + CH_3 + H, CH_4	28	
		88	**C_7H_4** + 2H, H_2	26	
	C_4H_2* + $CH_3C{\equiv}CD$ (C_7H_5D)	64	C_5H_2D + C_2H_3	??	acetylenic D retained, C_5H_4 interference
		63	C_5H_3 + C_2H_2D	4	acetylenic D lost
		64	**C_5H_4** + C_2HD	25−??	acetylenic D lost
		65	**C_5H_3D** + C_2H_2	16	acetylenic D retained
		75	**C_6HD** + CH_4	32	acetylenic D retained
		89	**C_7H_3D** + 2H, H_2	9	
	Other C_7 products have interference from deuterated impurities; assume 14%				
	C_4D_2* + $CH_3C{\equiv}CH$ ($C_7H_4D_2$)	63	**C_5H_3** + C_2HD_2	16	
		64	C_5H_2D + C_2H_2D	??	C_5H_4 interference
		65	**C_5H_3D** + C_2HD	37	one diacetylene D retained by C_5
		64	C_5H_4 + C_2D_2	6−??	includes C_5H_2D interference
		75	**C_6HD** + CH_3D	21	one diacetylene D retained by C_5
		76	C_6D_2 + CH_4		small; interference from C_4D_2* + C_4D_2
	C_7 products have interference from deuterated impurities; assume ~26%				
	C_4D_2* + $CH_3C{\equiv}CD$ ($C_7H_3D_3$)	64	**C_5H_2D** + C_2HD_2	12%	two methyl H's retained by C_5
		63	C_5H_3 + C_2D_3	none	
		65	C_5HD_2 + C_2H_2D	??	small; interference with C_5H_3D
		65	**C_5H_3D** + C_2D_2	18−??	all three methyl H's retained by C_5, interference with C_5D_2H
		66	**$C_5H_2D_2$** + C_2HD	15	two methyl H's retained by C_5
		67	C_5HD_3 + C_2H_2		none formed
		76	**C_6D_2** + CH_3D	29	interference with C_4D_2* + C_4D_2
	C_7 products have interference from deuterated impurities; assume ~26%				

[a] RC = reaction complex.

vibrational deactivator which overrides the effect of the change in buffer gas.

The most obvious trend in the rate constant data of Table 1 is the increase in the rate of the reaction with increasing C_nH_m size. In fact, this trend outweighs any differences in attack of C_4H_2* on double versus triple bonds.[29] The increasing reaction rate with increasing C_nH_m size may arise simply from the increased collision cross section for the C_4H_2* + C_nH_m pair.

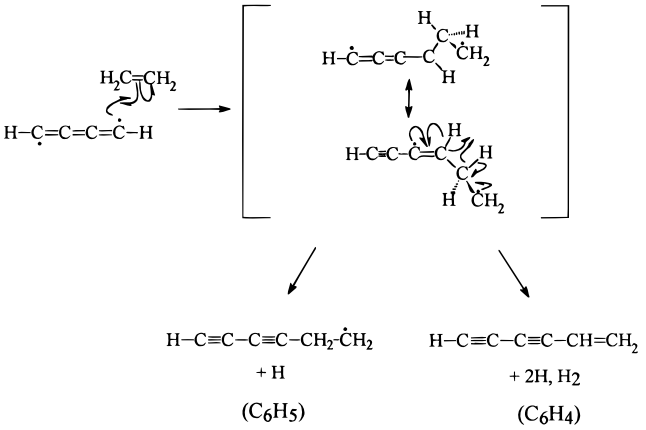

Figure 7. Proposed reaction mechanism for the $C_4H_2^* + C_2H_4$ reaction. The initially-formed reaction complex is shown in its two resonance forms in brackets. The reaction complex loses either one or two interior hydrogens to form the observed C_6H_5 or C_6H_4 reaction products. The mechanism accounts for the isotopic selectivity observed in the products of the $C_4H_2^* + C_2D_4$ and $C_4D_2^* + C_2H_4$ reactions.

C. Reaction Mechanisms. The isotopic data of Section IV.C were taken with the goal of probing the mechanism(s) of the $C_4H_2^* + C_nH_m$ reactions. The extensive *ab initio* calculations on the excited states of C_4H_2 by Karpfen and Lischka[30] indicate that the $T_1(^3\Sigma_u^+)$ and $T_2(^3\Delta_u)$ states of C_4H_2 have the electronic structure of a cumulene diradical:

$$H-\dot{C}=C=C=\dot{C}-H$$

The minimum energy structure for both states is only slightly bent and the potential energy surface for bending through the linear configuration is quite flat. The electron energy loss spectra of Allan[31] have located these states at about 62 and 74 kcal/mol above the ground state, respectively.

In our earlier work on the $C_4H_2^*$ reaction with C_4H_2 and C_2H_2 we proposed a reaction mechanism involving attack of a cumulene radical center on the unsaturated bond(s) of the reacting partner. This reaction mechanism is sufficient to explain much of the reaction chemistry observed here, but needs refinement in certain cases, most notably, in explaining the C_5 products formed in the reactions with propene and propyne.

1. $C_4H_2^* + C_2H_4$. In the $C_4H_2^* + C_2H_4$ reaction, two major products are formed, C_6H_4 (+2H, H_2) and C_6H_5 (+H), with the C_6H_4 product about four times as intense as the C_6H_5 product. Strong isotopic selectivity is evident in the products of the $C_4H_2^* + C_2D_4$ and $C_4D_2^* + C_2H_4$ reactions. In the former reaction, the C_6D_3H product is formed almost exclusively, indicating loss of one C_4H_2 hydrogen and one ethylenic deuterium atom from the reaction complex. Similarly, in the $C_4D_2^* + C_2H_4$ reaction, the C_6H_3D product dominates, again following loss of one C_4D_2 deuterium and one C_2H_4 hydrogen from the reaction complex. This is precisely the same isotopic selectivity observed in our earlier study[23] of $C_4H_2^* + C_2D_2$ in which C_6HD was formed exclusively.

Figure 7 presents a reaction mechanism which accounts for this selectivity. As indicated earlier, the mechanism invokes attack of $C_4H_2^*$ from one of its radical centers on the ethylenic double bond, forming a C_6H_6 reaction complex which can subsequently decompose by loss of the two interior hydrogens (one from diacetylene and one from ethene) to form the C_6H_4 product. Since the present experiment only detects the hydrocarbon product, it cannot distinguish whether the two hydrogens come off as H atoms or as the H_2 molecule. The strong isotopic selectivity argues for significant barriers to H/D exchange within the $C_6H_nD_{6-n}$ reaction complex. The C_6H_4 product is predicted by this mechanism to be a closed-shell en-diyne compound.

The minor product channel, involving formation of C_6H_5 + H, shows strong isotopic selectivity (~5:1) toward loss of the *diacetylene* H or D from the $C_6H_nD_{6-n}$ reaction complex. Note that C_6D_4H + H is formed preferentially from $C_4H_2^* + C_2D_4$ while C_6H_4D + D is formed selectively in the $C_4D_2^* + C_2H_4$ reaction. From the point of view of the proposed reaction mechanism, one might have expected similar propensities for loss of either interior hydrogen from the reaction complex.

The reason for the isotopic selectivity is likely dynamic rather than energetic. The preferred C_6H_5 product (formed when the interior H from C_4H_2 is lost) has the structure

$$H-C\equiv C-C\equiv C-CH_2-\dot{C}H_2$$

while loss of the ethylenic interior hydrogen would produce the isomer shown below.

$$H-C\equiv C-\dot{C}=CH-CH=CH_2$$

One expects that the first isomer would be less stable (as a primary, unconjugated free radical) than the second, yet based on the isotopic data, it is the first isomer which is formed preferentially. The reaction dynamics may favor loss of the $C_4H_2^*$ hydrogen, but if so, the reason that it does so is not known at present.

2. $C_4H_2^*$ + Propene, Propyne: C_6 and C_7 Products. We noted earlier that the products formed in the $C_4H_2^*$ reaction with propene and propyne show strong similarities, with propene products shifted up by two mass units from those in propyne. Figure 8 presents the proposed reaction mechanism applied to the C_6 and C_7 products of the $C_4H_2^*$ reaction with propene. The isotopic studies are again entirely consistent with the proposed mechanism. The C_7 pathways for the propene and propyne reactions involve radical center attack on the terminal ethylenic or acetylenic carbon, followed by loss of the interior hydrogen atoms from the C_7H_8 and C_7H_6 reaction complexes, respectively.

When $C_4H_2^*$ attack is on the central carbon atom of propene, the C_6HD_3 (C_6H_3D) product dominates the $C_4H_2^* + CD_3$-$CD{=}CD_2$ ($C_4D_2^* + CH_3CH{=}CH_2$) reaction. Loss of interior CD_3 + H (CH_3 + D) accompanies this channel, and the methyl radical products are detected by the VUV photoionization. What is not known is whether intact CH_4 is also produced in this channel. The C_6 products formed in the C_4H_2 reaction with propyne are formed in analogous pathways.

3. $C_4H_2^*$ + Propene, Propyne: C_5 Products. Mechanisms like those in Figures 7 and 8 cannot explain the C_5 products observed in the reactions with propene and propyne. Fortunately, the isotopic selectivity of the products formed from the isotopically labeled reactants provides significant constraints on any mechanism put forward (Table 2). Table 3 condenses the results of the isotopic studies into the smallest number of reaction pathways which account for all the major isotopic products of both reactions. The pathways posed for the C_5H_3 products assume that they are formed from the same reaction intermediates that lead to C_5H_4 products.

Mechanisms consistent with the conclusions of the isotopic studies are presented in Figure 9 for the reaction with propyne and Figure 10 for the reaction with propene. In all cases, initial attack occurs at the terminal unsaturated carbon of the C_3 reactant. If the adduct **1** undergoes a 1,5-hydrogen shift to form

(29) Unpublished data from our group on the $C_4H_2^*$ + 1,3-butadiene reaction confirm this trend, yielding a rate constant 1.27 ± 0.2 times that of $C_4H_2^* + C_4H_2$.

(30) Karpfen, A.; Lischka, H. *Chem. Phys.* **1986**, *102*, 91.
(31) Allan, M. *J. Chem. Phys.* **1984**, *80*, 6020.

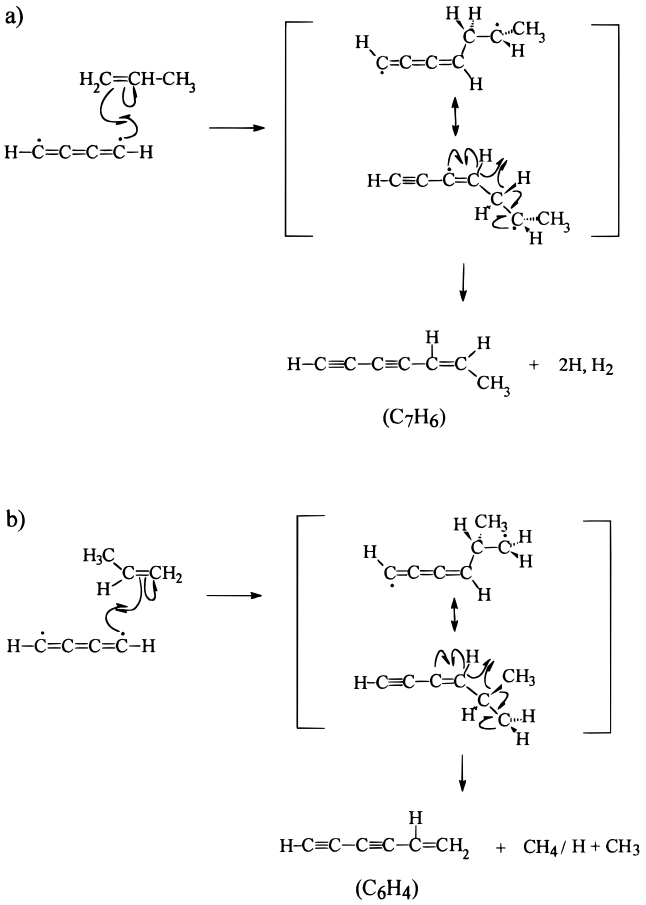

Figure 8. Proposed reaction mechanism for the C_6 and C_7 products of the C_4H_2* + propene reaction. The initially-formed reaction complex is drawn in its two resonant forms inside the brackets. (a) C_4H_2* attack on the terminal vinylic carbon forms C_7 products following loss of the interior hydrogen atoms from the reaction complex. (b) Attack on the interior carbon forms C_6 products following loss of either CH_4 or H + CH_3 from the reaction complex.

Table 3. Summary of the Isotopic Data on the C_5 Products from C_4H_2* + Propene, Propyne

$C_4H_2{}^{a}$* + $CH_3{}^{c}C{\equiv}CH^{b}$	→ $C_5H^{a}H_2{}^{c}H^{b}$	Scheme 1
	→ $C_5H_2{}^{c}H^{b}$	
$C_4H_2{}^{a}$* + $CH_3{}^{c}C{\equiv}CH^{b}$	→ $C_5H^{a}H_3{}^{c}$	Scheme 2
	→ $C_5H^{a}H_2{}^{c}$	
$C_4H_2{}^{a}$* + $CH_3{}^{c}CH^{b}{=}CH_2{}^{b}$	→ $C_5H_1H_2{}^{c}H_3{}^{b}$	Scheme 1
	→ $C_5H_2{}^{c}H_3{}^{b}$	
		No Scheme 2

2, either $H^{a}C{\equiv}CH^{c}$ loss can occur from one end to produce the C_5H_4 isomer **3** or 2,5-ring closure can form **5** followed by $H^{a}C{\equiv}CH^{b}$ expulsion to produce **6**. The route to **3** has precedence in the ultraviolet photochemistry of acrylonitrile, $H_2C{=}CH{-}C{\equiv}N$, which dissociates to HCN + $H_2C{=}C$: following ultraviolet excitation.[31] Rearrangement of **3** to **4** will likely follow during stabilization of the C_5H_4 product, though whether this rearrangement occurs on the time scale of our experiment cannot be determined from the present data. Note that **4** is the same isomer as **6**, but with different hydrogen content consistent with Scheme 1 of Table 3 rather than Scheme 2. This may account for the similar propensities for the two sets of products observed from the isotopic studies.

If enough energy is available to **3**, it can further decompose to C_5H_3 + H by loss of the vinylic hydrogen H^{a} which originated from diacetylene, resulting in a $C_5H_2{}^{c}H^{b}$ product, again as required for Scheme 1. The preference for loss of this hydrogen

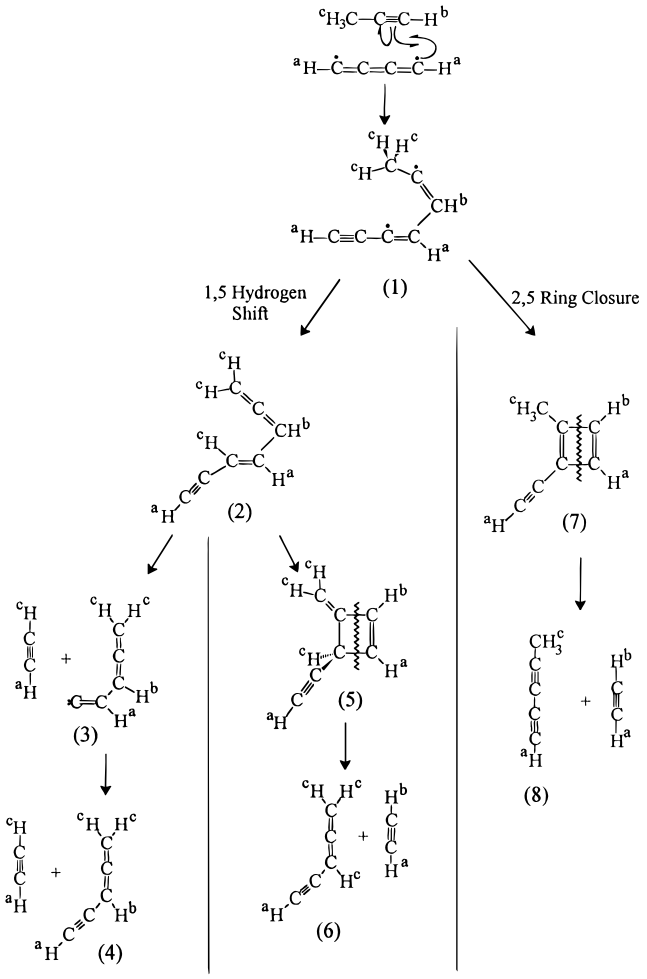

Figure 9. Proposed reaction mechanism for the formation of C_5H_4 + C_2H_2 products from the reaction of C_4H_2* + CH_3C_2H. The mechanism is consistent with the observed results of the deuteration studies from Table 3. Acetylene loss from the reaction complex occurs following (i) 2,5-ring closure, (ii) 1,5-hydrogen shift, or (iii) 2,5-ring closure subsequent to the 1,5-hydrogen shift.

is the same one noted earlier; namely, the loss of the interior hydrogen which originates from the metastable diacetylene. In the C_5H_4 product **6**, the weakest C-H bond involves the interior hydrogen, which upon dissociation yields the $C_5H^{a}H_2{}^{c}$ product.

As shown in Figure 9, a second route to the C_4H_2* + propyne products of Scheme 2 (Table 3) is open to adduct **1** which bypasses the 1,5-hydrogen shift. In that case **1** directly undergoes 2,5 ring closure, which after rearrangement of the double bonds in the cyclobutadiene moiety produces **7**. This is an anti-aromatic intermediate which is nevertheless estimated[32] to be about 10 kcal/mol lower in energy than **1**, so that there are no energetic constraints to its formation. Intermediate **7** can decompose to **8** by loss of $H^{a}C{\equiv}C{-}H^{b}$ to form the $C_5H_3{}^{c}H^{a}$ product. Here the $C_5H_2{}^{c}H^{a}$ + H^{c} product can be formed by subsequent loss of one of the methyl hydrogens to once again form the same isomeric product predicted by the other routes to C_5H_3. Note that **8** is a different C_5H_4 isomer than either **4** or **6**.

Finally, Figure 10 presents the analogous mechanisms applied to the C_4H_2* + propene reaction. Note that the routes involving 2,5 ring closure cannot produce C_5 products. Following the

(32) The heat of formation of cyclobutadiene is calculated to be 94.4 kcal/mol. See: Kollmar, J.; Carrion, F.; Dewar, M. J. S.; Bingham, R. C. *J. Am. Chem. Soc.* **1981**, *103*, 5292. Thus, $2C_2H_2$ → cyclobutadiene has $\Delta H_{rxn} = -14.6$ kcal/mol.

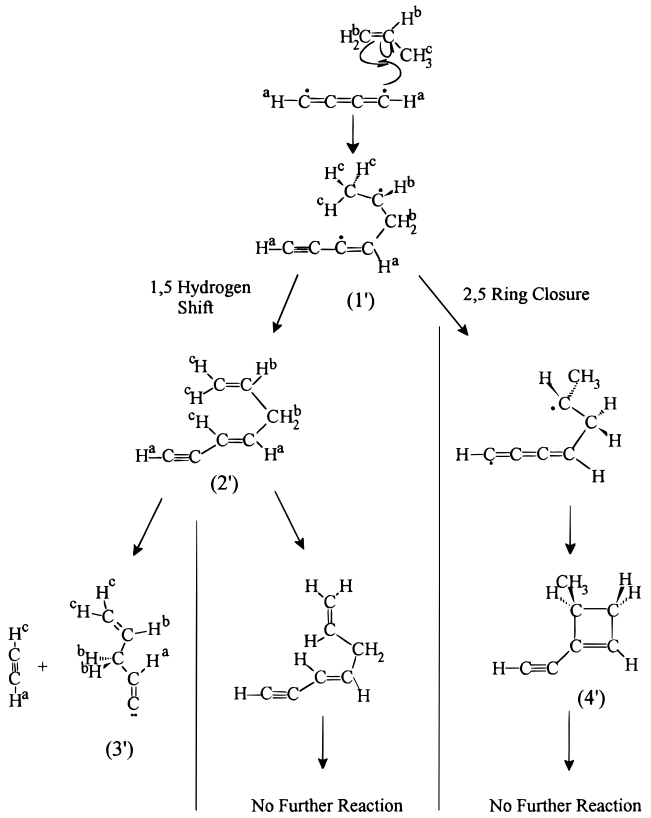

Figure 10. Proposed reaction mechanisms consistent with the conclusions of the isotopic studies for the formation of $C_5H_6 + C_2H_2$ in the reaction $C_4H_2^* + CH_3CH{=}CH_2$. As is evident from the mechanism, neither route in Scheme 2 can lead to C_5H_6 formation due to the increased saturation of the CH_3CHCH_2 reactant, consistent with Table 3. See text for further explanation.

1,5 hydrogen shift, ring closure cannot occur from **2′**. Ring closure from **1′** produces a cyclic butene which cannot expel C_2H_2 due to the lack of unsaturation in the cyclic intermediate **4′** formed. Only the route involving $H^aC{\equiv}CH^c$ loss from **2′** is open, and this route forms products from Scheme 1 of Table 3.

In summary, the proposed mechanisms can account for (i) the formation of C_5H_6/C_5H_5 products from the propene reaction in an analogous manner to the C_5H_4/C_5H_3 products from the propyne reaction, (ii) the deduction from the isotopic studies that the C_5H_6 product retains one and only one diacetylenic hydrogen, and (iii) the experimental finding that only Scheme 1 is open in the reaction with propene while both Schemes 1 and 2 are open to the $C_4H_2^* +$ propyne reactants.

VI. Conclusion

The reactions of metastable $C_4H_2^*$ with ethene, propene, and propyne have produced a wide range of larger, highly unsaturated hydrocarbon products. Reaction mechanisms have been put forward which correctly account for the observed isotopic data, but clearly, spectroscopic conformation of these products is still needed.

Quenching data on $C_4H_2^*$ is required before quantitative modeling of metastable C_4H_2 reactions occurring in Titan's atmosphere and in flames can be carried out. In particular, it will be of interest to compare the rates and products of the $C_4H_2^*$ reactions with those from $C_4H + C_nH_m$. Preliminary estimates of the importance of $C_4H_2^*$ chemistry using the quenching of metastable acetylene[33] as a guide indicate that in the lower stratosphere of Titan, the $C_4H_2^*$ reactions could play a role comparable to that of C_4H or C_2H in forming larger hydrocarbon products.

The qualitative result of this work is that $C_4H_2^* + C_nH_m$ chemistry produces a set of unusual conjugated-chain molecules and radicals which may themselves undergo interesting further chemistry both in flames and in Titan's atmosphere.

Acknowledgment. The authors gratefully acknowledge support from the NASA Planetary Atmospheres program for this research. They also acknowledge many helpful discussions with G. B. Ellison and R. R. Squires regarding the mechanisms of these reactions. Finally, the microsphere plate ion detector used in this work was donated by El-Mul Technologies.

JA953757C

(33) Zwier, T. S.; Allen, M. Unpublished results.